Abatement of the antibiotic levofloxacin in a solar photoelectro-Fenton flow plant: Modeling the dissolved organic carbon concentration-time relationship

Gabriela Coria[a], Tzayam Pérez[b], Ignasi Sirés[c, **], Enric Brillas[c], José L. Nava[a, *]

[a] Universidad de Guanajuato, Departamento de Geomática e Hidráulica, División de Ingenierías, Av. Juárez 77, Col. Centro, C.P. 36000 Guanajuato, Gto, Mexico
[b] Universidad de Guanajuato, Departamento de Ingeniería Química, División de Ciencias Naturales y Exactas, Norial Alta S/N, C.P. 36050 Guanajuato, Gto, Mexico
[c] Laboratori d'Electroquímica dels Materials i del Medi Ambient, Departament de Química Física, Facultat de Química, Universitat de Barcelona, Martí i Franquès 1-11, 08028 Barcelona, Spain

ABSTRACT

The degradation of solutions of the antibiotic levofloxacin (LVN) in sulfate medium at pH 3.0 has been investigated at pre-pilot scale by solar photoelectro-Fenton (SPEF) process. The flow plant included an FM01-LC filter-press cell equipped with a Ti|Pt anode and a three-dimensional-like air-diffusion cathode, connected to a compound parabolic collector as photoreactor and a continuous stirred tank under recirculation batch mode. The effect of volumetric flow rate on H_2O_2 electrogeneration from O_2 reduction was assessed. Then, the influence of initial LVN concentration and Fe^{2+} concentration as catalyst on dissolved organic carbon (DOC) removal was thoroughly investigated. LVN was gradually mineralized by SPEF process, with faster DOC abatement at 0.50 mM Fe^{2+}, yielding 100% after 360 min at applied cathodic potential of -0.30 V|SHE. The high mineralization current efficiency (MCE) and low specific energy consumption (EC_{DOC}) revealed the extraordinary role of homogeneous hydroxyl radicals and natural UV light, which allowed the degradation of the antibiotic and its by-products with MCE values greater than 100%. Five cyclic by-products, *N,N*-dimethylformamide and up to three short-chain linear carboxylic acids were detected by GC-MS and HPLC analyses. A parametric model to simulate the DOC decay versus electrolysis time was implemented for the SPEF pre-pilot flow plant, showing good agreement with experimental data.

© 2017.

1. Introduction

Quinolones are broad-spectrum antibacterial drugs and, in modern therapeutics, almost all of them belong to the class of fluoroquinolones. Levofloxacin (LVN, see structure in Table 1) is one of the most popular fluorinated quinolones, being used for the treatment of infectious diseases like pneumonia and abdominal infections (Mandell et al., 2007; Nasuhoglu et al., 2012; El Najjar et al., 2013; Epold et al., 2015). The occurrence of antibiotics in water bodies as a result of their massive and uncontrolled use has raised serious concerns worldwide due to the proliferation of antibiotic-resistant bacteria, so-called superbugs, which are responsible for killing an estimated 700,000 people each year (Willyard, 2017). Therefore, it is urgent to develop more efficient treatments to transform the antibiotics into less active and more biodegradable molecules (Michael et al., 2013; Blair et al., 2015; Brillas and Sirés, 2015). The ability of several advanced oxidation processes (AOPs) to remove LVN from water has been recently investigated, including ozonation (Witte et al., 2009), photocatalysis (Sturini et al., 2012), conventional Fenton (Wang et al., 2016) and sonochemical AOPs (Guo et al., 2010; Wei et al., 2015). These methods are characterized by the in-situ production of hydroxyl radical (

$^{\bullet}$OH) at ambient conditions, giving rise to effective, efficient, safe and eco-friendly treatments that may allow the complete mineralization of the organic matter (Dirany et al., 2012; Oturan and Aaron, 2014).

Among the electrochemical AOPs, the performance of electro-Fenton (EF) process with carbon felt and activated fiber cathodes to degrade LVN has been recently reported (Gong et al., 2016; Yahya et al., 2016; Liu et al., 2017). In general, these systems allowed a fast decay of LVN concentration and a final mineralization >90% at 360–480 min. However, current efficiencies were very low, attaining 40–50% as maximum (Yahya et al., 2016; Liu et al., 2017). In EF with large 3D-like cathodes, Fenton's reagent (Fe^{2+} + H_2O_2) can be continuously generated upon two-electron reduction of gaseous or dissolved O_2 by reaction (1) and monoelectronic conversion of Fe^{3+} to Fe^{2+} by reaction (2), thus yielding large amounts of free $^{\bullet}$OH in the bulk from Fenton's reaction (3) at optimum pH near 3 (Sirés et al., 2014; Sopaj et al., 2015; Lanzalaco et al., 2017).

$$O_{2(g)} + 2 H^+ + 2 e^- \rightarrow H_2O_2 \tag{1}$$

$$Fe^{3+} + e^- \rightarrow Fe^{2+} \tag{2}$$

$$H_2O_2 + Fe^{2+} \rightarrow Fe^{3+} + {}^{\bullet}OH + OH^- \tag{3}$$

* Corresponding author.
** Corresponding author.
Email addresses: i.sires@ub.edu (I. Sirés); jlnm@ugto.mx (J.L. Nava)

Table 1

Intermediates identified by GC-MS during the SPEF treatment of solutions of 6 L of 60 mg L^{-1} DOC of LVN (**1**) with 0.050 M Na$_2$SO$_4$ and 0.50 mM Fe^{2+} at pH = 3.0 and volumetric flow rate = 3.0 L min^{-1}. Potential applied to the GDE employed as cathode (E_{cath}) = −0.30 V|SHE.
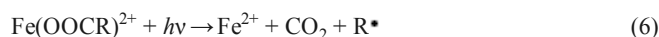
Number	Chemical name	Molecular structure	t_r[a] (min)	Main fragmentation ions (m/z)
1	Levofloxacin		−	
2	N,N-Diethylformamide		5.8	101, 86, 72, 58, 44
3	1-Methyl-2-pyrrolidone		11.2	99, 71, 56, 41
4	2-Phenoxyethanol		16.5	138, 107, 94, 77
5	1H-Indole-2,3-dione (Isatin)		19.1	147, 104, 76, 50
6	4-Oxo-1,4-dihydroquinoline-3-carboxylic acid		24.4	189, 173, 143, 89
7	2-Fluoro-5-nitrophenol		27.7	157, 127, 111, 83

[a] Retention time.

In undivided electrolytic cells, adsorbed hydroxyl radicals (M(•OH)) are formed at the surface of active and non-active anodes (M) from water oxidation via reaction (4) (Panizza and Cerisola, 2009; Labiadh et al., 2016). Hence, organic molecules are destroyed by both, free •OH and adsorbed M(•OH), although the former radical has much higher oxidation ability to promote combustion (Sirés et al., 2014; Martínez-Huitle et al., 2015).

$$M + H_2O \rightarrow M(\bullet OH) + H^+ + e^- \quad (4)$$

The decontamination treatment can be significantly accelerated by illuminating the solution with UVA light from either a commercial lamp in photoelectro-Fenton (PEF) or natural sunlight in solar PEF (SPEF). This high energy radiation causes the photoreduction reaction (5) that transforms the main Fe(III) species at acidic pH into Fe^{2+}, as well as the photolysis of some refractory intermediates. A good example of this latter phenomenon is the photodecarboxylation of stable complexes of linear carboxylic acids with Fe(III) from reaction (6) (Sirés et al., 2014; Martínez-Huitle et al., 2015).

$$Fe(OH)^{2+} + h\nu \rightarrow Fe^{2+} + \bullet OH \quad (5)$$

$$Fe(OOCR)^{2+} + h\nu \rightarrow Fe^{2+} + CO_2 + R\bullet \quad (6)$$

In previous works, we have shown some of the interesting features of the SPEF approach to efficiently degrade pesticides (Flox et al., 2007a, b), pharmaceuticals (Pérez et al., 2017), dyes (Thiam et al., 2015) and industrial additives (Flox et al., 2007a,b; Steter et al., 2018). On the other hand, we have studied the cathodic two-electron reduction of oxygen at different carbonaceous substrates, highlighting that graphite felt enhances the H$_2$O$_2$ electrogeneration owing to its large volumetric area (Coria et al., 2015).

Within the chemical engineering field, several studies have been devoted to modeling the degradation of persistent organic pollutants upon application of AOPs (Royaee and Sohrabi, 2012). In contrast, modeling of SPEF treatment of organic contaminants is rather limited, which is mainly due the very recent demonstration of its great potential. In particular, in a previous work we described, for the first time, a mathematical model to simulate the treatment in a SPEF flow plant. The suggested parametric model to simulate the dissolved organic carbon (DOC) decay of erythromycin versus time showed a good agree-

ment between experimental and theoretical data (Pérez et al., 2017). In such mathematical model, the reaction term implemented to the compound parabolic collector (CPC) used as photoreactor obeyed a zero-order kinetics because of the complex formula of erythromycin having 37 carbon atoms. However, the robustness of our mathematical model needs to be verified for other molecules.

This manuscript reports a study on the SPEF treatment of acidic synthetic solutions of LVN in a pre-pilot flow plant of 6 L capacity. The plant arrangement included an FM01-LC filter-press cell equipped with a Ti|Pt anode and an air-diffusion cathode. The reactor was connected in series with a CPC and a continuous stirred tank (CST). The influence of catalyst and LVN concentrations on the degradation rate, mineralization current efficiency and energy consumption for total mineralization was assessed. Higher drug concentrations than those found in the aquatic environment were tested aiming to know the oxidation ability of the SPEF process. The simulation of DOC decay versus time was performed by using the aforementioned parametric model. The evolution of intermediates was followed by chromatographic techniques.

2. Experimental

2.1. Reagents

All the chemicals used in this study were of analytical grade and were used without further purification. LVN (purity 98%) was obtained from Sigma Aldrich. Heptahydrate ferrous sulfate (purity 99%), anhydrous sodium sulfate (purity 99%), sulfuric acid and sodium hydroxide were supplied from J.T Baker and Fermont. Chromatographic grade acetonitrile and formic acid were purchased from Sigma-Aldrich. Synthetic solutions were prepared with deionized water.

2.2. Flow plant

2.2.1. Description of the SPEF plant

Fig. SM-1 shows the setup of the SPEF pre-pilot plant that combines an FM01-LC filter-press reactor in series with a CPC photoreactor and a mixing tank that contains 6 L of solution. The plant was operated under recirculation batch mode. The undivided electrochemical reactor was equipped with a platinized Ti plate anode (64 cm^2), which was made following the Pechini method, and an unmodified graphite felt pressed on top of carbon cloth as air-diffusion cathode (0.15 cm thickness, 64 cm^2 cross sectional area). The carbon cloth and graphite felt were provided by ROOE Group. The dry face of the cathode was in contact with an air chamber fed with atmospheric air under overpressure regulated with a back-pressure gauge to continuously electrogenerate H$_2$O$_2$ from reaction (1). A Dewalt® D55168 air compressor was used for air feeding at a constant pressure of 0.5 psi. The characteristics of the FM01-LC reactor are shown in Table SM-1 and a sketch can be found elsewhere (Rivera et al., 2015). The CPC photoreactor was rigorously designed and constructed by ourselves (Pérez et al., 2017).

2.2.2. Methodology for the tests in the SPEF plant

Prior to mineralization experiments, H$_2$O$_2$ was electrogenerated into a 0.050 M Na$_2$SO$_4$ solution for 1 h in the dark (i.e., using an opaque cloth to cover the CPC). In our previous communication Coria et al. (2015), the analysis of the polarization curves revealed that the two-electron reduction of oxygen at graphite felt in sulfate medium occurred under mass transport control within the cathodic

potential (E_{cath}) domain of $-0.4 < E < -0.1$ V vs the standard hydrogen electrode (SHE). The best accumulation H$_2$O$_2$ in the present SPEF flow pant operating in the same range of E_{cath} at volumetric flow rate (q) of 3.0 L min^{-1} was achieved at -0.30 V|SHE, achieving a concentration of 120 mg L^{-1} in 6 L of solution. Solutions containing different concentrations of LVN and Fe^{2+} catalyst in 0.050 M Na$_2$SO$_4$ at pH 3.0 were then treated at this optimum E_{cath}. The potentiostatic electrolyses were performed with a BK Precision® 1621 A power source, which directly displayed the potential difference between the electrodes (E_{cell}, in V). The electrode potentials were measured against a saturated sulfate reference electrode, inserted into a Luggin capillary, using an Agilent® 34,410 high impedance multimeter. All electrode potentials in this work are referred to SHE. The SPEF trials were carried out for 360 min in sunny days during the autumn of 2017. The average daily UV solar irradiance (from 300 to 400 nm) was measured by a weather station located at the University of Guanajuato, yielding ~55 W m^{-2}.

2.2.3. Formulation of the numerical simulation of the SPEF plant

In a previous paper, Pérez et al. (2017) described in detail the characteristics and considerations of the mathematical model employed to simulate the DOC decay in the SPEF flow plant. This model allows determining the global apparent reaction term of the DOC in the solution, separating the contribution of the non-ideal flow deviations in the FM01-LC and CPC photoreactor. However, the experimental DOC abatement during the mineralization of LVN presented a pseudo-second order kinetics (see below), which differed from the published pseudo-first order kinetics for erythromycin. Therefore, a brief description of the mathematical model is given below with attention to the reaction term associated with DOC decay.

The 1D differential model employs the dispersion mass balance for the FM01-LC, the dispersion mass balance with a global reaction rate term for the CPC, and the mass balance at the CST in transient regime. Considering C_0 as the DOC value at the CST outlet, C_1 the DOC value of the solution at the FM01-LC and C_2 the solution DOC inside the CPC that feeds the CST, the differential mass balance at the FM01-LC at electrolysis time t omitting reaction terms is:

$$\frac{\partial C_1}{\partial t} = D_{ax1}\frac{\partial^2 C_1}{\partial y^2} - \frac{U_{01}}{\varepsilon}\frac{\partial C_1}{\partial y} \tag{7}$$

where D_{ax1} is the axial dispersion coefficient to quantify the non-ideal flow deviations such as the retro-mixing degree, U_{01} is the mean inflow velocity at the inlet of the FM01-LC and ε accounts for the graphite felt porosity.

The mass balance at the CPC includes the reaction term via a global mineralization rate that accounts for the oxidation of LVN and its by-products by homogeneous •OH in the bulk:

$$\frac{\partial C_2}{\partial t} = D_{ax2}\frac{\partial^2 C_2}{\partial x^2} - U_{02}\frac{\partial C_2}{\partial x^2} - k_{app}C_2{}^n \tag{8}$$

where D_{ax2} is the axial dispersion coefficient, U_{02} is the mean inflow velocity at the CPC inlet, k_{app} is the apparent global kinetic constant and n is the reaction order. For LVN, $n = 2$, as will be discussed later.

The differential mass balance within the CST without any reaction term is:

$$\frac{\partial C_0}{\partial t} = \frac{q}{V_T}\left(C_2\left(t,L\right) - C_0\right)$$

$$(9)$$

where V_T is the reservoir volume, q is the volumetric flow rate, t is the electrolysis time in the recycle operation mode, and L is the axial position at the exit of the CPC reactor.

Eqs. (7)–(9) were solved using the boundary conditions described elsewhere (Pérez et al., 2017). Table SM-2 summarizes the transport parameters and electrolyte properties employed in the simulation performed. The mass balance Eqs. (7)–(9) were solved via finite element method using COMSOL Multiphysics® 5.1 package considering 42,300 lineal elements. A computer with a 2.6 GHz processor and 16 GB of RAM was employed. Simulation run times lasted for 40 s and the numerical error was below 0.001% with time steps of 1 min and an absolute tolerance of 0.001.

2.3. Analytical procedures

The solution pH was determined with a Hanna HI991300 pH-meter. The H_2O_2 concentration was determined from the light absorption of the colored complex with Ti(IV) at $\lambda = 408$ nm (Welcher, 1975), measured on a Perkin Elmer Lambda 35 UV/Vis spectrophotometer. The mineralization of LVN solutions was followed from their DOC abatement, determined on a Tekmar Torch TOC analyzer. Generated carboxylic acids were detected by ion-exclusion HPLC using a Perkin Elmer Flexar LC fitted with an Agilent Hi-Plex H 8 mm, 300 mm × 7.7 mm (i.d.), column at room temperature and coupled with a Flexar photodiode array detector set at $\lambda = 210.0$ nm. These measurements were performed by injecting 20 μL samples into the LC and using a 4 mM H_2SO_4 solution as mobile phase at 0.6 mL min^{-1}. Ion exclusion chromatograms exhibited peaks related to oxalic, maleic and formic acids at retention times of 9.2, 13.8 and 17.6 min, respectively. Ion chromatographic analysis of nitrate and fluoride was carried out by injecting 100 μL aliquots into the above LC, equipped with a Hamilton PRP-X110, 150 mm × 4.1 mm (i.d.), anion-exchange column at room temperature and coupled to an Adept Cecil CE4710 conductivity detector. A mixture of 4 mM p-hydroxybenzoic acid, 0.1 mM NaSCN and 2.5% methanol at pH 8.5 was eluted at 1.5 mL min^{-1} as mobile phase. The ammonium concentration was determined spectrophotometrically (Pérez et al., 2017).

Intermediates formed at 60 and 120 min of the SPEF treatment of 60 mg L^{-1} DOC of LVN solutions at $E = -0.30$ V|SHE were identified by GC-MS. About 100 mL aliquots were extracted out with 3 × 25 mL of CH_2Cl_2. The organic phase was reduced to about 1 mL once dried over anhydrous Na_2SO_4. GC-MS analysis of concentrated samples was made by employing an Agilent system (Steter et al., 2018). NIST05-MS library allowed the interpretation of the resulting mass spectra.

3. Results and discussion

3.1. Effect of catalyst concentration on the SPEF treatment under potentiostatic conditions

In a first series of experiments, 0.28 mM LVN solutions (60 mg L^{-1} DOC) with 0.050 M Na_2SO_4 and different concentrations of Fe^{2+} catalyst between 0.50 and 0.70 mM were comparatively degraded by SPEF at pH 3.0 and $q = 3.0$ L min^{-1} for 360 min. These trials were performed at E_{cath} of -0.30 V|SHE in order to ensure a constant H_2O_2

production with minimum H_2 evolution reaction (HER), as explained in section 2.2.2.

Fig. 1a illustrates the depletion of DOC concentration with time for these experiments. According with several previous works on Fenton-based electrochemical processes carried out with air-diffusion cathodes, the mineralization rate is enhanced at an optimum Fe^{2+} concentration of 0.50 mM. This can be explained by the greater production of $^{\bullet}OH$ in the bulk from Fenton's reaction (3) (Sirés et al., 2014; Brillas and Martínez-Huitle, 2015; Brillas and Sirés, 2015). This concentration was also found as optimal for the SPEF degradation of LVN, yielding 100% mineralization after 360 min (see Fig. 1a). In contrast, further increase to 0.60 and 0.70 mM Fe^{2+} caused a decelera-
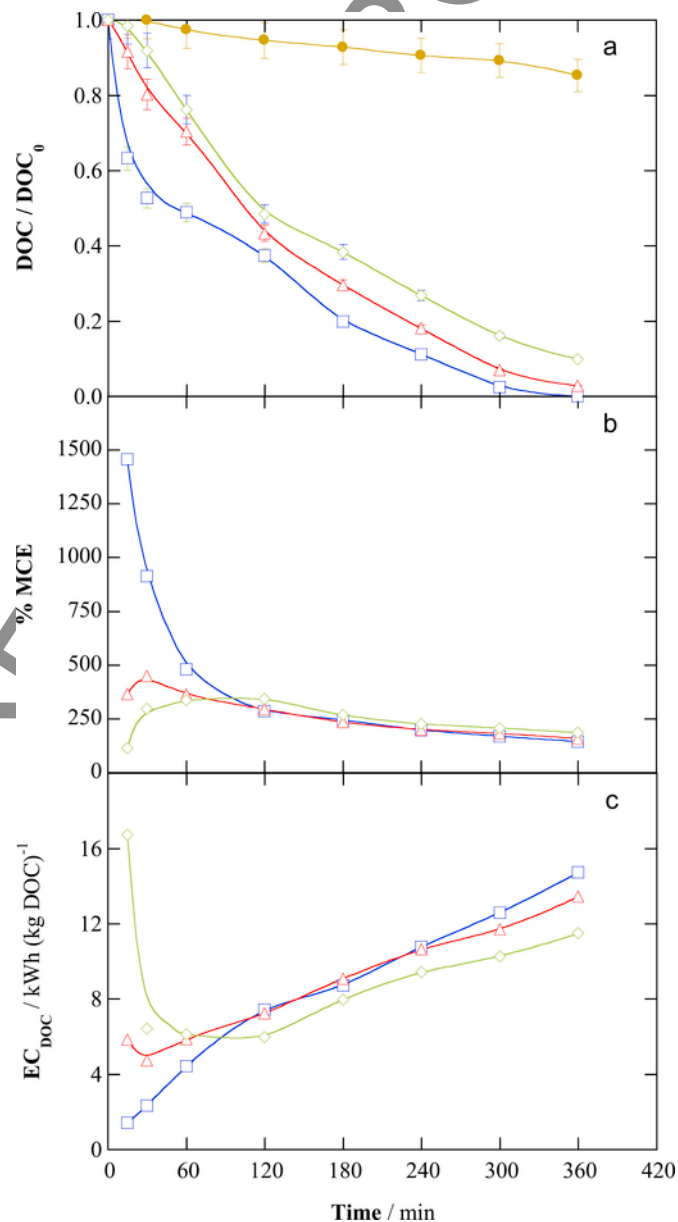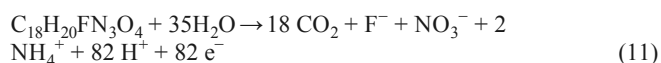

Fig. 1. Variation of (a) normalized DOC, (b) mineralization current efficiency and (c) specific energy consumption per kilogram of DOC with electrolysis time for the SPEF treatments at different Fe^{2+} concentrations: (□) 0.50, (△) 0.60 and (◇) 0.70 mM. Treated solution: 6 L of 60 mg L^{-1} DOC of LVN with 0.050 M Na_2SO_4 at pH 3.0. Volumetric flow rate $q = 3.0$ L min^{-1}. Potential applied to the cathode (E_{cath}) = -0.30 V|SHE. In (a), (●) no addition of Fe^{2+}.

tion in DOC abatement, leading to partial mineralization within the same time period. This is attributed to the parasitic reaction (10), which causes the consumption of •OH by the excess of Fe^{2+} ion added, eventually limiting the oxidation power of the SPEF process.

$$Fe^{2+} + \text{•OH} \rightarrow Fe^{3+} + OH^- \qquad (10)$$

The great oxidation ability of SPEF was demonstrated by performing a test in the absence of Fe^{2+} catalyst (so-called electro-oxidation with H_2O_2). As depicted in Fig. 1a, a very poor mineralization of ca. 15% was achieved after 360 min. This informs about the much lower oxidation power of adsorbed Pt (•OH) formed at the Ti|Pt anode via reaction (4) compared to free •OH, because it is well known that platinum or platinized anodes are considered as active electrodes (Panizza and Cerisola, 2009; El-Ghenymy et al., 2014).

Taking into account that the complete electrochemical combustion of LVN yielded NH_4^+, NO_3^- and F^- as major ions, as will be discussed below, the mineralization reaction can be described as follows:

$$C_{18}H_{20}FN_3O_4 + 35H_2O \rightarrow 18\ CO_2 + F^- + NO_3^- + 2\ NH_4^+ + 82\ H^+ + 82\ e^- \qquad (11)$$

Despite 82 mol of protons were produced per mol of LVN, the solution pH remained almost constant because they are simultaneously consumed during H_2O_2 electrosynthesis from reaction (1). The mineralization current efficiency (MCE, in %) for the transformation of the total mass of carbon (m, in g) per mol of LVN contained in the solution volume ($V_S = 6$ L) upon supply of n mol of electrons (= 82) was then assessed from the experimental DOC abatement ($\Delta(DOC)_{exp}$, in $g\,L^{-1}$):

$$\frac{\%MCE = nF\,V_s\,\Delta(DOC)_{exp} \times 100}{m\,Q_t} \qquad (12)$$

where F is the Faraday constant (96,487 $C\,mol^{-1}$) and Q_t is the applied charge at each time (in C). On the other hand, the specific energy consumption per unit DOC mass (EC_{DOC}) was calculated as:

$$EC_{DOC}\left(kWh(kgDOC)^{-1}\right) = \frac{2.7 \times 10^{-4}\,E_{cell}\,Q_t}{V_s\,\Delta(DOC)_{exp}} \qquad (13)$$

where 2.7×10^{-4} is a conversion factor for units homogenization.

Fig. 1b confirms that 0.50 mM Fe^{2+} was the optimum catalyst concentration not only to provide a fast and total decontamination by SPEF, but also to make it in the most efficient manner. The trial at 0.50 mM Fe^{2+} attained the greatest MCE values, reaching an impressive maximum near 1500% at short electrolysis time. Such high values arise from: (i) the low electrical consumption required to run the electrolyses, with a small E_{cath} of -0.30 V|SHE being sufficient to efficiently produce H_2O_2 (Coria et al., 2015), and (ii) the crucial contribution of photochemical reactions (5) and (6) promoted by sunlight, which allow the destruction of refractory complexes in concomitance with a continuous photoregeneration of Fe^{2+} catalyst as it is converted to Fe^{3+} from reaction (3). Although to a much smaller extent, these reasons are also valid for SPEF treatment with 0.60 and 0.70 mM Fe^{2+}, attaining maximum MCE values of 450% and 350%, respectively. On the other hand, note that the treatment became progressively less efficient as the electrolyses were prolonged. This re-

sulted from the slower DOC removals caused by the smaller organic matter load in solution and its change into a much more refractory mixture of by-products and complexes with Fe(III).

On the contrary, Fig. 1c shows that the energy consumption became smaller as the oxidation power of the system was enhanced, particularly evident during the first 60 min. Total mineralization at 360 min using 0.50 mM Fe^{2+} only required an EC_{DOC} ~15 kWh (kg DOC)$^{-1}$.

3.2. Effect of levofloxacin concentration on the SPEF treatment

Considering the best catalyst concentration of 0.50 mM Fe^{2+}, another series of experiments was performed by treating solutions of 6 L with different DOC concentrations within the range 30–60 $mg\,L^{-1}$ in 0.050 M Na_2SO_4 at pH 3.0, $q = 3.0\,L\,min^{-1}$ and $E_{cath} = -0.30$ V|SHE. Fig. 2a shows that the complete mineralization of LVN at a concentration of 30 $mg\,L^{-1}$ DOC was achieved at 180 min, whereas a longer time of 360 min was needed at concentrations between 40 and 60 $mg\,L^{-1}$ DOC (Fig. 2b–d). In addition, the mineralization rate decreased at growing LVN concentration, as expected from the slower removal of more numerous organic molecules due to the action of a constant concentration of oxidants and photon flux in all cases. An analysis in terms of kinetic rate constants supports this assumption (see below). However, the MCE profiles collected in Fig. 3a indicate an opposite behavior, since the highest efficiencies were obtained for the treatment at 60 $mg\,L^{-1}$ and then the values decreased slightly as the initial DOC concentration was reduced to 30 $mg\,L^{-1}$. These results suggest that the role of parasitic reactions (10), (14) and (15) became less relevant at higher organic matter concentration, once the oxidizing radicals could encounter the organic molecules more easily (Sirés et al., 2014; Brillas and Martínez-Huitle, 2015). Worth mentioning, the MCE was above 100% during all the electrolysis under all conditions.

$$2\,\text{•OH} \rightarrow H_2O_2 \qquad (14)$$

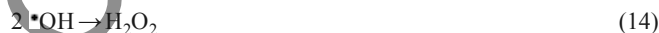$$H_2O_2 + \text{•OH} \rightarrow HO_2\text{•} + H_2O \qquad (15)$$

Fig. 3b shows the corresponding energy consumption per kg of DOC for the same experiments. The highest consumption was obtained for the experiment at 30 $mg\,L^{-1}$ DOC, gradually requiring less energy as the initial DOC was increased. Anyway, the EC_{DOC} needed for complete mineralization was always within the range of ~15–20 kWh (kg DOC)$^{-1}$, which is very low compared to energy consumed to abate other organic pollutants like erythromycin by SPEF (Pérez et al., 2017).

3.3. Comparison of the parametric model with experimental data

Fig. 2 shows the theoretical DOC-time curves as solid lines determined from the proposed parametric model, along with experimental data discussed above for initial DOC of 30, 40, 50 and 60 $mg\,L^{-1}$ (0.14–0.28 mM LVN). The values of the pseudo-second-order kinetic constants (k) determined according to the model were 6.5, 6.0, 1.2, and 0.8 $M^{-1}\,s^{-1}$, respectively. Theoretical and experimental data show close agreement for 30 and 40 $mg\,L^{-1}$ DOC concentration. For the experiments at higher concentrations, with a slower kinetics, the quality of the fitting decreased, probably due to the larger accumulation of recalcitrant intermediates that could not be mineralized quickly and then interfered.

The proposed model is useful for the assessment of the global apparent reaction term, in which •OH is considered to have the main
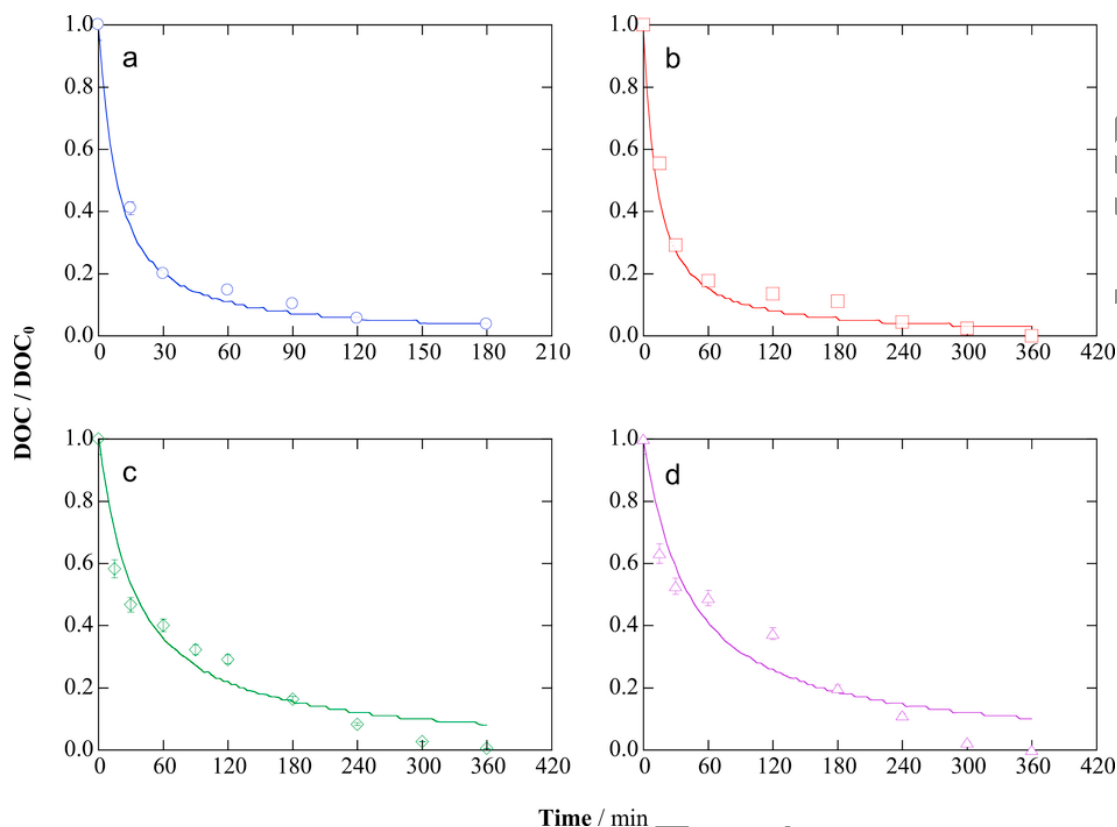
Fig. 2. Normalized DOC decay versus electrolysis time for the SPEF treatments of 6 L of different initial LVN concentrations: (a, ○) 30, (b, □) 40, (c, ◇) 50 and (d, △) 60 mg L^{-1} DOC of LVN with 0.050 M Na$_2$SO$_4$ and 0.50 mM Fe^{2+} at pH = 3.0. Volumetric flow rate q = 3.0 L min^{-1}. Potential applied to the cathode (E_{cath}) = −0.30 V|SHE. Solid lines (—) are the theoretical data trends determined from the parametric model considering C_0 as initial DOC. Error bars within 95% confidence interval are provided.

role during cold combustion. In the model, the •OH concentration is presupposed to be constant, always considering a constant sunlight radiation and constant H$_2$O$_2$ production. However, in practice, during the 360 min of electrolysis there were variations in solar radiation, which might induce stochastic deviations in the experimental DOC points. It is worth mentioning that the linear regression coefficients were comprised between $0.83 \le R^2 \le 0.97$. We consider that these values are acceptable in such complex SPEF process, where mainly the irregular sunlight radiation induce some behavior that is difficult to simulate. This confirms the necessity to implement a more robust model that includes the effect of sunlight radiation, as well as the dependence of H$_2$O$_2$ production with current density.

3.4. Identification and time course of intermediates and released inorganic ions

Table 1 summarizes the cyclic and aliphatic intermediates determined by GC-MS analysis. These by-products may be formed by the combined action of hydroxyl radicals, which cause the gradual hydroxylation of some C and N atoms, and UV light. Simultaneous cleavage of the piperazine and benzene rings of LVN (**1**) yielded the aliphatic amide **2** or, alternatively, the pyrrolidone **3** via internal cyclization. If all the side bonds of the parent benzene ring except the C—O are broken, 2-phenoxyethanol (**4**) is formed. Isatin (**5**) appeared upon internal cyclization as well, once the piperazine ring was cleaved, but with the benzene ring maintaining its original integrity. Simultaneous cleavage of all side C—F, C—N and C—O bonds of (**1**) yielded 4-oxo-1,4-dihydroquinoline-3-carboxylic acid (**6**). Finally, fluorinated derivative (**7**) was formed upon attack of hydroxyl radi-

cals. Note that all by-products previously reported by Yahya et al. (2016) and Liu et al. (2017) under electro-Fenton conditions displayed larger molar masses, and they did not discuss their potential transformation into other cyclic derivatives like those described here prior to complete ring cleavage.

Considering the subsequent fragmentation of by-products **2**–**7**, the electrolyzed solutions were analyzed by ion-exclusion HPLC in order to identify linear short-chain aliphatic carboxylic acids. The chromatograms exhibited well defined peaks for oxalic, formic and maleic acids. Fig. 4a shows a great accumulation of formic acid, reaching a maximum value of 95 mg L^{-1} at 90 min of electrolysis, which corresponds to 25 mg L^{-1} DOC. According to Fig. 1a, only 45% of initial DOC (i.e., 27 mg L^{-1} DOC) remained in solution at 90 min, which means that most of the organic matter at that time was formic acid. The acid concentration diminished from that time until it completely disappeared at 360 min. The concentration of oxalic and maleic acids was always much smaller, attaining 1.28 and 12 mg L^{-1}, respectively.

Fig. 4b shows the time course of inorganic ions formed during the SPEF treatment of LVN. Nitrate and fluoride were the accumulated anions, whereas ammonium was formed as cation, as shown in reaction (11). A quick accumulation can be observed for NO$_3^-$ and F$^-$ up to steady concentrations of 12.0 mg L^{-1} (0.19 mM) and 5.2 mg L^{-1} (0.28 mM, 100% of initial F), respectively, reached at about 60 min as a result of the cleavage of **1**, by-products **2**–**7** and, possibly, some other unidentified intermediates upon action of •OH, Pt (•OH) and UV light. A more gradual accumulation was obtained for ammonium, finally attaining 8.1 mg L^{-1} (0.45 mM, practically twice of that NO$_3^-$) at 360 min. The sum of nitrate + ammonium ions accounted for by
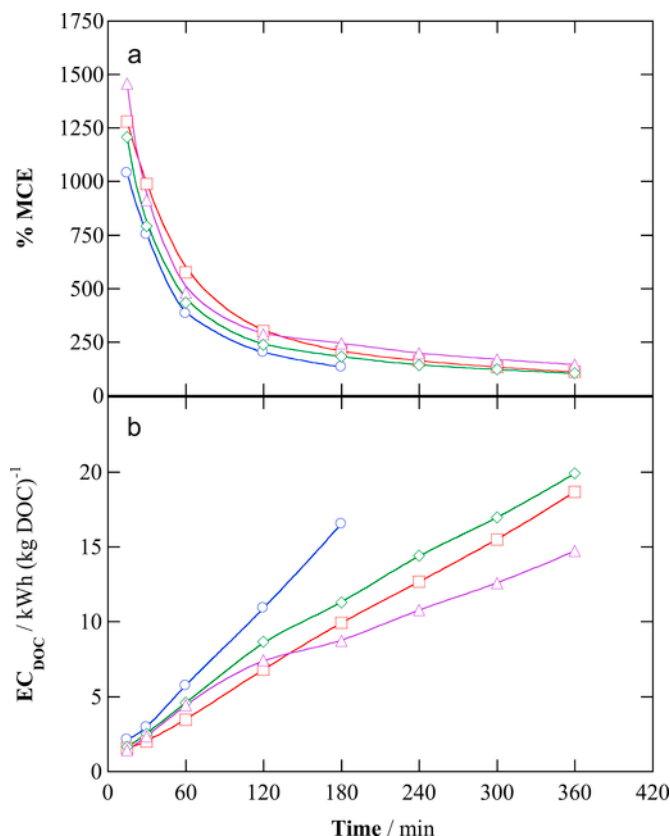
Fig. 3. (a) Mineralization current efficiency and (b) specific energy consumption per kilogram of DOC as a function of the electrolysis time for the SPEF treatments of Fig. 2.

Fig. 4. (a) Evolution of the concentration of (◇) formic, (○) maleic and (□) oxalic acids detected during the SPEF treatment of 6 L of a 60 mg L^{-1} DOC of LVN (0.28 mM) solution with 0.050 M Na$_2$SO$_4$ and 0.50 mM Fe^{2+} at pH = 3.0, q = 3.0 L min^{-1} and E_{cath} = −0.30 V|SHE. (b) Time course of the concentration of released (×) NH$_4^+$, (△) NO$_3^-$ and (▽) F$^-$ ions.

76% of initial N contained in LVN and hence, some volatile *N*-species were plausibly formed during the electrolyses (Thiam et al., 2015).

4. Conclusions

SPEF treatments performed at constant E_{cath} = −0.30 V|SHE ensured the best H$_2$O$_2$ production, so that LVN solutions in sulfate medium at pH 3.0 were completely mineralized in a very efficient manner in a pre-pilot plant equipped with an FM01-LC filter-press reactor. A catalyst concentration of 0.50 mM Fe^{2+} was found as optimal to maximize the formation of •OH in the bulk from Fenton's reaction, whereas UV light from natural sunlight was efficiently collected in the CPC photoreactor to allow the photodecomposition of mainly refractory complexes of organic by-products with Fe(III). Parasitic reactions were minimized as the initial LVN concentration was increased, reaching an impressive MCE ~1500% at short electrolysis time at 60 mg L^{-1} DOC. In all cases, low energy consumptions of ~15–20 kWh (kg DOC)$^{-1}$ were required to attain complete DOC removal. A parametric model assessing the global apparent kinetic constants for DOC decay, assuming •OH as the main oxidant and ignoring the contribution of dispersion flow deviations in both reactors, was validated under potentiostatic conditions with good agreement between experimental and predicted data. Five cyclic derivatives along with *N,N*-diethylformamide and three short-chain linear carboxylic acids, with predominance of formic acid, were formed during the degradation. The initial N and F atoms were released as NH$_4^+$, NO$_3^-$ and F$^-$ ions.
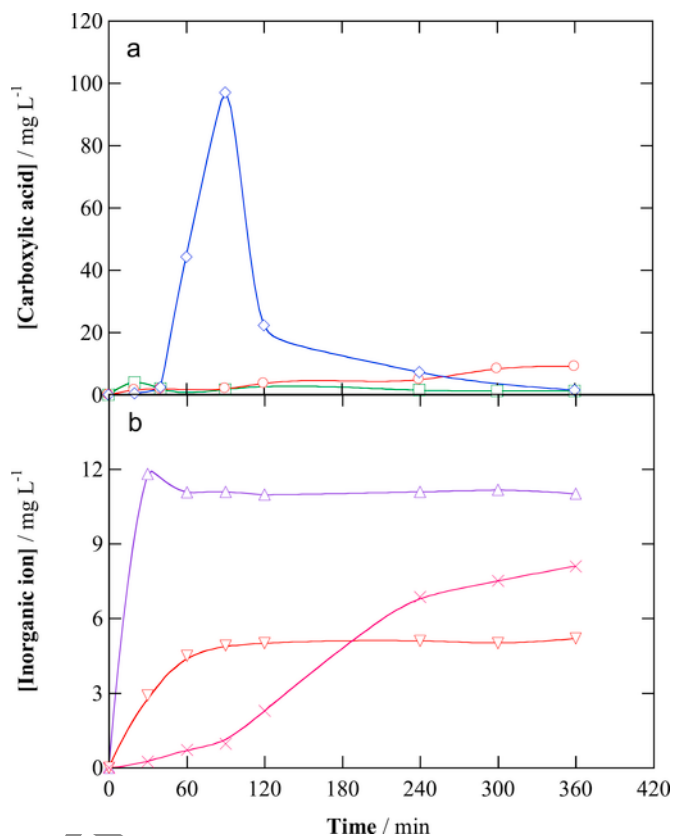
Appendix A. Supplementary data

Supplementary data related to this article can be found at https://doi.org/10.1016/j.chemosphere.2018.01.112.

Uncited reference

Brillas et al., 2000.

References

Blair, B., Nikolaus, A., Hedman, C., Klaper, R., Grundl, T., 2015. Evaluating the degradation, sorption, and negative mass balances of pharmaceuticals and personal care products during wastewater treatment. Chemosphere 134, 395–401.

Brillas, E., Calpe, J.C., Casado, J., 2000. Mineralization of 2,4-D by advanced electrochemical oxidation processes. Water Res. 34, 2253–2262.

Brillas, E., Martínez-Huitle, C.A., 2015. Decontamination of wastewaters containing synthetic organic dyes by electrochemical methods. An updated review. Appl. Catal. B Environ. 166–167, 603–643.

Brillas, E., Sirés, I., 2015. Electrochemical removal of pharmaceuticals from water streams: reactivity elucidation by mass spectrometry. Trac. Trends Anal. Chem. 70, 112–121.

Coria, G., Pérez, T., Sirés, I., Nava, J.L., 2015. Mass transport studies during dissolved oxygen reduction to hydrogen peroxide in a filter-press electrolyzer using graphite felt, reticulated vitreous carbon and boron-doped diamond as cathodes. J. Electroanal. Chem. 757, 225–229.

Dirany, A., Sirés, I., Oturan, N., Özcan, A., Oturan, M.A., 2012. Electrochemical treatment of the antibiotic sulfachloropyridazine: kinetics, reaction pathways, and toxicity evolution. Environ. Sci. Technol. 46, 4074–4082.

El-Ghenymy, A., Rodríguez, R.M., Brillas, E., Oturan, N., Oturan, M.A., 2014. Electro-Fenton degradation of the antibiotic sulfanilamide with Pt/carbon-felt and BDD/carbon-felt cells. Kinetics, reaction intermediates, and toxicity assessment. Environ. Sci. Pollut. Res. 21, 8368–8378.

El Najjar, N.H., Touffet, A., Deborde, M., Journel, R., Leitner, N.K., 2013. Levofloxacin oxidation by ozone and hydroxyl radicals: kinetic study, transformation products and toxicity. Chemosphere 93, 604–611.

Epold, I., Trapido, M., Dulova, N., 2015. Degradation of levofloxacin in aqueous solutions by Fenton, ferrous ion-activated persulfate and combined Fenton/persulfate systems. Chem. Eng. J. 279, 452–462.

Flox, C., Cabot, P.L., Centellas, F., Garrido, J.A., Rodríguez, R.M., Arias, C., Brillas, E., 2007a. Solar photoelectro-Fenton degradation of cresols using a flow reactor with a boron-doped diamond anode. Appl. Catal. B Environ. 75, 17–28.

Flox, C., Garrido, J.A., Rodríguez, R.M., Cabot, P.L., Centellas, F., Arias, C., Brillas, E., 2007b. Mineralization of herbicide mecoprop by photoelectro-Fenton with UVA and solar light. Catal. Today 129, 29–36.

Gong, Y., Li, J., Zhang, Y., Zhang, M., Tian, X., Wang, A., 2016. Partial degradation of levofloxacin for biodegradability improvement by electro-Fenton process using an activated fiber felt cathode. J. Hazard Mater. 304, 320–328.

Guo, W., Shi, Y., Wang, H., Yang, H., Zhang, G., 2010. Intensification of sonochemical degradation of antibiotics levofloxacin using carbon tetrachloride. Ultrason. Sonochem. 17, 680–684.

Labiadh, L., Barbucci, A., Carpanese, M.P., Gadri, A., Panizza, M., 2016. Comparative depollution of Methyl Orange aqueous solutions by electrochemical incineration using TiRuSnO₂, BDD and PbO₂ as high oxidation power anodes. J. Electroanal. Chem. 766, 94–99.

Lanzalaco, S., Sirés, I., Sabatino, M.A., Dispenza, C., Scialdone, O., Galia, A., 2017. Synthesis of polymer nanogels by electro-Fenton process: investigation of the effect of main operation parameters. Electrochim. Acta 246, 812–822.

Liu, X., Yang, D., Zhou, Y., Zhang, J., Luo, L., Meng, S., Chen, S., Tan, M., Li, Z., Tang, L., 2017. Electrocatalytic properties of N-doped graphite felt in electro-Fenton process and degradation mechanism of levofloxacin. Chemosphere 182, 306–315.

Mandell, L.A., Wunderink, R.G., Anzueto, A., 2007. Infectious Diseases Society of America/American Thoracic Society consensus guidelines on the management of community-acquired pneumonia in adults. Clin. Infect. Dis. 44, S27–S72.

Martínez-Huitle, C.A., Rodrigo, M.A., Sirés, I., Scialdone, O., 2015. Single and coupled electrochemical processes and reactors for the abatement of organic water pollutants: a critical review. Chem. Rev. 115, 13362–13407.

Michael, I., Rizzo, L., McArdell, C.S., Manaia, C.M., Merlin, C., Schwartz, T., Dagot, C., Fatta-Kassinos, D., 2013. Urban wastewater treatment plants as hotspots for the release of antibiotics in the environment: a review. Water Res. 47, 957–995.

Nasuhoglu, D., Rodayan, A., Berk, D., Yargeau, V., 2012. Removal of the antibiotic levofloxacin (LEVO) in water by ozonation and TiO₂ photocatalysis. Chem. Eng. J. 189–190, 41–48.

Oturan, M.A., Aaron, J.-J., 2014. Advanced oxidation processes in water/wastewater treatment: principles and applications. A review. Crit. Rev. Environ. Sci. Technol. 44, 2577–2641.

Panizza, M., Cerisola, G., 2009. Direct and mediated anodic oxidation of organic pollutants. Chem. Rev. 109, 6541–6569.

Pérez, T., Sirés, I., Brillas, E., Nava, J.L., 2017. Solar photoelectro-Fenton flow plant modeling for the degradation of the antibiotic erythromycin in sulfate medium. Electrochim. Acta 228, 45–56.

Rivera, F.F., Ponce de León, C., Walsh, F.C., Nava, J.L., 2015. The reaction environment in a filter-press laboratory reactor: the FM01-LC flow cell. Electrochim. Acta 161, 436–452.

Royaee, S.J., Sohrabi, M., 2012. Comprehensive study on wastewater treatment using photo-impinging streams reactor: residence time distribution and reactor modeling. Ind. Eng. Chem. Res. 51, 4152–4160.

Sirés, I., Brillas, E., Oturan, M.A., Rodrigo, M.A., Panizza, M., 2014. Electrochemical advanced oxidation processes: today and tomorrow. A review. Environ. Sci. Pollut. Res. 21, 8336–8367.

Sopaj, F., Rodrigo, M.A., Oturan, N., Podvorica, F.I., Pinson, J., Oturan, M.A., 2015. Influence of the anode materials on the electrochemical oxidation efficiency. Application to oxidative degradation of the pharmaceutical amoxicillin. Chem. Eng. J. 262, 286–294.

Steter, J.R., Brillas, E., Sirés, I., 2018. Solar photoelectro-Fenton treatment of a mixture of parabens spiked into secondary treated wastewater effluent at low input current. Appl. Catal. B Environ. 224, 410–418.

Sturini, M., Speltini, A., Maraschi, F., Profumo, A., Pretali, L., Irastorza, E.A., Fasani, E., Albini, A., 2012. Photolytic and photocatalytic degradation of fluoroquinolones in untreated river water under natural sunlight. Appl. Catal. B Environ. 119–120, 32–39.

Thiam, A., Sirés, I., Brillas, E., 2015. Treatment of a mixture of food color additives (E122, E124 and E129) in different water matrices by UVA and solar photoelectro-Fenton. Water Res. 81, 178–187.

Wang, L., Zhao, Q., Hou, J., Yan, J., Zhang, F., Zhao, J., Ding, H., Li, Y., Ding, L., 2016. One-step solvothermal synthesis of magnetic Fe₃O₄-graphite composite for Fenton-like degradation of levofloxacin. J. Environ. Sci. Health A 51, 52–62.

Wei, H., Hu, D., Su, J., Li, K., 2015. Intensification of levofloxacin sono-degradation in a US/H₂O₂ system with Fe₃O₄ magnetic nanoparticles. Chin. J. Chem. Eng. 23, 296–302.

sixth ed., Welcher, F.J. (Ed.), 1975. Standard Methods of Chemical Analysis, vol. 2, R.E. Krieger Pub. Co, Huntington, New York, p. 1827, (Part B).

Willyard, C., 2017. The drug-resistant bacteria that pose the greatest health threats. Nature 543, 15.

Witte, B.D., Langenhove, H.V., Hemelsoet, K., Demeestere, K., Wispelaere, P.D., Van Speybroeck, V., Dewulf, J., 2009. Levofloxacin ozonation in water: rate determining process parameters and reaction pathway elucidation. Chemosphere 76, 683–689.

Yahya, M.S., El Karbane, M., Oturan, N., El Kacemi, K., Oturan, M.A., 2016. Mineralization of the antibiotic levofloxacin in aqueous medium by electro-Fenton process: kinetics and intermediate products analysis. Environ. Technol. 37, 1276–1287.